

Robotic Surface Finishing Processes: Modeling, Control, and Experiments

Prabhakar R. Pagilla

Assistant Professor
e-mail: pagilla@ceat.okstate.edu

Biao Yu

Graduate Student

School of Mechanical
and Aerospace Engineering,
Oklahoma State University,
Stillwater, OK 74078-5016

Control of robotic surface finishing processes such as deburring, grinding, chamfering, and polishing is considered in this paper. A complete dynamic model that describes the dynamic behavior of the robot for surface finishing tasks is developed. A complete surface finishing task is divided into three phases (free motion phase, transition phase, and constrained motion phase) depending on the location of the robot end-effector with respect to the constraint surface. Stable control algorithms are developed for each phase. Emphasis is given to the transition phase and constrained motion phase, where surface finishing takes place. An experimental platform for performing robotic surface finishing operations is developed. The robotic surface finishing system consists of a planar robot with a force sensor and a deburring tool on its end-effector, and a fixture to hold the constraint surface. Extensive experiments based on the proposed control design were conducted for both surface following and surface finishing. Results of surface following and surface finishing experiments are shown and discussed. [DOI: 10.1115/1.1344881]

1 Introduction

Conventional machine tools, such as CNC operated, are used in general to remove a large amount of material to shape a part to its desired geometry. Finishing of the machined part is required to remove material in small amounts to bring the part to the required tolerance. In addition to small material removal, localized burr formations have to be removed. Examples of these surface finishing operations are grinding, deburring, and chamfering. These operations constitute a significant portion of effort and money in the manufacturing industry. Automation of such processes is still in its rudimentary stages.

It is known that material finishing operations such as deburring, grinding, chamfering and other edge finishing operations can be responsible for 10–30 percent of all manufacturing costs [1–3]. A burr is formally defined as an “undesirable projection of material formed as a result of plastic flow from a cutting, forming, blanking or shearing operation” [1]. Even with the present state of technology in manufacturing, problems of burr removal are still encountered by manufacturers. This is mainly due to the fact that in most manufacturing plants deburring is performed by human labor, which is highly labor intensive [1]. Annual deburring costs alone are currently estimated at \$3.9 billion nationwide [4]. These costs include time required to finish a part at the bench, the cost of thorough inspection, possible subsequent rework, and sometimes rejection of the component. In a recent assessment of critical Pratt & Whitney needs in technology development, it was revealed that the problem of deburring and finishing ranked second in a list of 46 manufacturing problems.

Automation of surface finishing operations is an active area of investigation in the manufacturing industry and also in several national laboratories, including the National Institute of Standards and Technology and Sandia National Laboratories [5,6,4]. Research toward automation has focused in many directions from prediction and modeling of burr formation [7] to creating intelligent machines [8,9] for such operations. Several important research problem areas have been pointed out in [1,2,6,8]. Accurate position and force control of the robot in the presence of uncertainties and stable transition between free motion and contact mo-

tion were reported to be some of the major factors that need to be addressed to create an advanced deburring system. The development of a passive one-degree-of-freedom end-effector force control system for efficient deburring was demonstrated in [7]. In [8] experimental results for robotic deburring of two-dimensional parts using an impedance control method have been shown. Deburring using force control and active end-effector system has been presented in [9].

An essential component for successful automation of surface finishing process is appropriate control of the mechanical system to achieve required performance, such as specified surface finish to hold tolerances, precision contours, and tool-workpiece integrity. Effective controller design requires knowledge of several items: (i) accurate modeling of the mechanical system to model the behavior of the system interacting with the external environment during the process, (ii) knowledge of the process model, such as cutting force models and burr models. Also, controller design should be robust to uncertainties in both the system and process models.

Considerable research in the theory of constrained mechanical systems has been reported in the last decade. Some of the early work on simultaneous position and force control of robot manipulators was done in [10–12]. The motivation for some of this early work was to make progress towards automation of manually performed manufacturing operations. Precise positioning of the robot relative to the workpiece is required for efficiently performing these operations. Force feedback is often used to compensate for positioning inaccuracies. Control algorithms that emerged in this area during the 80's and 90's can be broadly classified into three categories: hybrid position/force control [12,13]; impedance control [14,15]; and constrained mechanical systems modeled as differential-algebraic equations [16–19]. Much of the research conducted using the three approaches has been based on the assumption that the robot is already in contact with the external environment. This is truly not the case in many industrial applications, as the robot moves in free space before making contact with the workpiece. In most machining applications the surface is rigid. Consequently switching from free motion to constrained motion on the workpiece surface can cause significant stability problems due to non-zero velocity of impact. The transition from free motion to constrained motion leads to impact forces on the system and results in discontinuities in system equations.

Some recent research in the constrained mechanical systems

Contributed by the Dynamic Systems and Control Division for publication in the JOURNAL OF DYNAMIC SYSTEMS, MEASUREMENT, AND CONTROL. Manuscript received by the Dynamic Systems and Control Division October 4, 1999. Associate Editor: Y. Hurmuzlu.

area has focused on several solutions to deal with contact transitions. Stability of task transition for robots has been considered in [20], where the transitions are assumed to take place smoothly, and the surface is modeled as a compliant environment. A dimensionless representation of the impact behavior was developed in [21], and an integral force feedback was used to improve the transient impact response. A discontinuous contact transition control algorithm for mechanical systems subject to a unilateral constraint was developed in [22]. Force regulation and contact transition control of robots has been considered in [23], where measurement of acceleration is assumed in the controller design. Recent results in modeling and control of mechanical systems subject to unilateral constraints can be found in [24]. Control laws for the regulation case in the presence of contacts and impacts among parts of mechanical systems is considered in [25]. The effect of the presence of inequality constraints on the behavior of a linear continuous-time dynamical system is investigated from a system theoretic point of view in [26]. Mechanical systems with geometric inequality constraints are complementarity systems [27,28]. A critical study of the applicability of rigid-body collision theory was done in [29]. Impact phenomena is discussed via experimental analysis using a dropped bar onto an external surface.

A typical automated surface finishing process involves the following sequence: the robot starts from the home position and moves freely for some time, makes contact with the workpiece, follows the workpiece contour while removing material and burrs from the surface, and leaves the surface returning to home position. For complex contours with disconnected segments on the same workpiece to be machined, the robot has to leave and make contact with the workpiece several times. It is typical in the surface finishing operation that the part to be machined has very high stiffness. If the robot impacts the part with a non-zero velocity, there is a possibility of bouncing behavior. It is essential to minimize these bounces during transition and to maintain stability of the robot for the entire operation.

In this paper a model for the dynamics of a robot performing a complete surface finishing task is developed. The dynamic model includes three phases of motion: free motion phase, transition phase, and constrained motion phase. A new stable discontinuous transition control algorithm is proposed for the transition phase. The constrained motion phase involves motion control along the tangential directions of the surface that is to be machined and force control in the normal directions. Further, the dynamics involves tangential forces due to the material removal. At steady feed-rate (velocity tangential to the surface) the normal force magnitude and tangential force magnitude are related by coefficient of grinding friction [30]. Since the coefficient of grinding friction is not known exactly, an estimation algorithm is designed to estimate it. Experiments using the proposed controller were conducted for both surface following and surface finishing.

The rest of the paper is organized as follows. In Section 2, we describe the dynamic model of a robot for surface finishing operations. Control algorithms for each phase of the complete task is developed in Section 3. Section 4 gives a description of the experimental platform. Experimental results of surface following and surface finishing are discussed in Section 5. Conclusions and future research are given in Section 6.

2 Robot Dynamic Model for Surface Finishing Operations

Let the kinetic and potential energy functions of an n -link robot be given by $\mathcal{K}(q, \dot{q}) = 1/2 \dot{q}^T M(q) \dot{q}$ and $\mathcal{P}(q)$, where (q, \dot{q}) are the generalized position and velocity, respectively, and $M(q) \in \mathbb{R}^{n \times n}$ is the symmetric positive definite mass matrix. The dynamics of the robot is given by

$$M(q)\ddot{q} + C(q, \dot{q})\dot{q} + g(q) = \tau + J^T(q)f \quad (1)$$

where $C(q, \dot{q})$ is the matrix composed of Coriolis and centripetal terms, $g(q)$ is the gravity vector, τ is the vector of generalized

forces applied by the motors at each joint of the robot, f represents the vector of external forces, and $J(q)$ is the Jacobian of the manipulator. Let the geometric constraint on the robot be modeled by the following unilateral constraint,

$$\phi(x(q)) \leq 0, \quad (2)$$

where $x(q)$ is the Cartesian position. The constraint is assumed to be smooth. Define the following orthogonal projection matrix whose image represents the normal direction of the constraint,

$$P_\phi(q) = \left(\frac{\partial \phi}{\partial q} \right) \left(\frac{\partial \phi}{\partial q} \right)^T / \left\| \left(\frac{\partial \phi}{\partial q} \right) \right\|^2$$

and the kernel of $P_\phi(q)$ gives the tangential direction of the constraint, and is given by

$$Q_\phi(q) = I - P_\phi(q)$$

where $\|x\|$ denotes the 2-norm of x . The external force, f , given in (1) is the contact force due to the constraint, and can be written as

$$f = n(x)f_n + t(x)f_t \quad (3)$$

where $n(x)$ and $t(x)$ represent the unit normal and tangential directions of the constraint surface, respectively, in the Cartesian space, and f_n and f_t represent the normal force and tangential force magnitudes, respectively. The value of the contact force, $\|f\|$, depends on the activation/deactivation of the constraint,

$$\phi(q) < 0 \Rightarrow \|f\| = 0 \quad (4)$$

$$\phi(q) = 0 \Rightarrow \|f\| \geq 0 \quad (5)$$

A complete task of the robot in the presence of the unilateral constraint can be divided into three phases: (a) when $\phi(q) < 0$, then the robot is said to be in free motion phase, (b) when $\phi(q) = 0$ and the velocity normal to the surface is zero, then the robot is said to be in the constrained motion phase, and (c) transition from free motion phase to constrained motion phase is termed as the transition phase. The presence of the unilateral constraint in the robot workspace divides the state space into the following sets:

$$X_c := \{q, \dot{q} \in \mathbb{R}^n : \phi(q) = 0\} \quad (6)$$

$$X_u := \{q, \dot{q} \in \mathbb{R}^n : \phi(q) < 0\} \quad (7)$$

$$X_f := \{q, \dot{q} \in \mathbb{R}^n : \phi(q) > 0\} \quad (8)$$

where X_c represents the configurations wherein the robot lies on the constraint surface, X_u represents configurations that the robot can freely move, and X_f represents the configurations that violate the constraint. The space X_c can be subdivided into the sets X_{ct} and X_{ca} , i.e., $X_c = X_{ct} \cup X_{ca}$, where

$$X_{ct} := \{q, \dot{q} \in \mathbb{R}^n : \phi(q) = 0, P_\phi(q)\dot{q} \neq 0\} \quad (9)$$

$$X_{ca} := \{q, \dot{q} \in \mathbb{R}^n : \phi(q) = 0, P_\phi(q)\dot{q} = 0\} \quad (10)$$

where $P_\phi(q)\dot{q}$ indicates the velocity normal to constraint surface. The motivation for this subdivision is that the system can impact the constraint surface with a nonzero normal velocity, and there is a jump condition in velocity. Notice that X_{ct} is the set of all impact points. The transition phase takes place when the robot jumps between X_{ct} and X_u . With the division of the robot workspace, the dynamics in each phase can be written as follows:

If $q \in X_u$ then the dynamic equations are

$$M(q)\ddot{q} + C(q, \dot{q})\dot{q} + g(q) = \tau \quad (11)$$

If $q \in X_c$, then the dynamic equations are

$$M(q)\ddot{q} + C(q, \dot{q})\dot{q} + g(q) = \tau + J^T(q)f \quad (12)$$

If $q \in X_{ct}$ then the jump condition for Eq. (12) is given by

$$\dot{q}_+ = \mathcal{D}(q, \dot{q}_-) \quad (13)$$

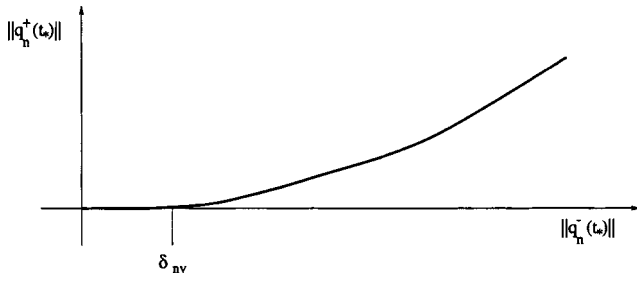


Fig. 1 Postimpact versus preimpact normal velocity

In Eq. (13), \dot{q}_+ and \dot{q}_- represent the impact velocity and the rebound velocity, respectively. $\mathcal{D}(\cdot)$ represents an operator which maps the impact velocity to the rebound velocity. This operator can take several forms depending on the choice of the impact model for the constraint surface. We assume that the magnitude of the preimpact normal velocity versus the postimpact normal velocity is related as shown in Fig. 1. In Fig. 1, $\dot{q}_n^-(t_*) = P_\phi \dot{q}_n^+(t_*)$, $\dot{q}_n^+(t_*) = P_\phi \dot{q}_n^-(t_*)$, and δ_{nv} represents a threshold normal impact velocity, below which the magnitude of the postimpact normal velocity is zero. For a mechanical linkage [31], it can be assumed that there is a finite amount of kinetic energy reduction during impact is given by

$$KE^+ - KE^- = -\Delta K < 0 \quad (14)$$

where $KE^- = 1/2[\dot{q}^-]^T M(q)[\dot{q}^-]$ and $KE^+ = 1/2[\dot{q}^+]^T M(q)[\dot{q}^+]$ are preimpact kinetic energy and postimpact kinetic energy, respectively. Impacts are generally treated as very large forces acting over a short duration of time. If impact occurs over an infinitesimally small period of time, then (i) all velocities remain finite and (ii) there is no change in position of the system [32,31]. If Δt is the duration of collision and $f(\omega)$ is impact force during collision, then the generalized force impulse F_I due to the impact at time t_* is given by

$$F_I = \lim_{\Delta t \rightarrow 0} \int_{t_*}^{t_* + \Delta t} J^T(q) f(\omega) d\omega. \quad (15)$$

Integrating (1), at the moment of impact we obtain

$$M(q) \Delta \dot{q}(t_*) = F_I \quad (16)$$

where $\Delta \dot{q}(t_*) = \dot{q}(t_*^+) - \dot{q}(t_*^-)$. The magnitude of the force impulse, F_I , depends on the preimpact velocity. Further, when there is tangential friction, the force impulse has components in the normal and tangential directions [3], i.e., $F_I = P_\phi F_I + Q_\phi F_I$. If frictionless impact is assumed then the force impulse lies in the normal direction only, i.e., $F_I = P_\phi F_I$.

It is known that when steady contact and feedrate (velocity along the constraint surface) is reached, f_n and f_t are related by the coefficient of grinding friction [30], which is,

$$f_t = \xi f_n \quad (17)$$

where ξ is the coefficient of grinding friction. Define

$$\begin{aligned} v(q) &= J^T(q) n(x): && \text{maps normal surface force magnitude} \\ &&& \text{into corresponding joint forces} \\ \bar{v}(q) &= v(q) / [v(q)^T v(q)] \\ v'(q) &= J^T(q) t(x): && \text{maps tangential surface force} \\ &&& \text{magnitude into corresponding} \\ &&& \text{joint forces} \end{aligned}$$

The robot dynamics during surface finishing process becomes

$$M(q) \ddot{q} + C(q, \dot{q}) \dot{q} + g(q) = \tau + v(q) f_n + v'(q) \xi f_n \quad (18)$$

The dynamics for a complete surface finishing task is summarized as follows.

- Free motion phase:

$$M(q) \ddot{q} + C(q, \dot{q}) \dot{q} + g(q) = \tau \quad (19)$$

- Transition phase:

$$M(q) \ddot{q} + C(q, \dot{q}) \dot{q} + g(q) = \tau \text{ and } \dot{q}_+ = \mathcal{D}(q, \dot{q}_-) \quad (20)$$

- Constrained motion phase:

$$M(q) \ddot{q} + C(q, \dot{q}) \dot{q} + g(q) = \tau + v(q) f_n + v'(q) \xi f_n \quad (21)$$

3 Control Design

For surface finishing operations, the control goal is to move the robot toward the surface, make contact with the surface, perform the designed operation, i.e., chamfering, deburring, polishing, etc., and leave the surface to return to the initial point. The desired path of the robot end-effector for this operation is shown as DABCD in Fig. 3. The paths DA, BC, and CD are pure motion trajectories. Along DA the normal velocity component decreases and becomes zero at point A. During path AB the robot end-effector follows the surface while applying a desired force normal to the surface.

The control goal in free motion phase is to track the desired motion trajectory considering manipulator model uncertainties. During constrained motion phase, the control goal is to simultaneously track the desired motion in tangential direction, regulate the desired force normal to the constraint surface. Switching directly to simultaneous motion and force control in the constrained motion could lead to severe repeated impact of the robot on the surface. A stable transition controller assures that repeated impacts do not occur. In the following control law for each phase is proposed.

3.1 Model-Based Adaptive Control for Free Motion.

During this phase the robot is in free motion. An experimentally well tested model based adaptive controller considering robot parameter uncertainties is chosen. The adaptive model-based control law and parameter adaptation law are

$$\tau = Y(q, \dot{q}, \ddot{q}_r, \ddot{q}_r) \hat{\beta}(t) - F_v e_v(t) \quad (22)$$

$$\hat{\beta}(t) = \beta_0 - \int_0^t \Gamma^{-T} Y^T(q, \dot{q}, \ddot{q}_r, \ddot{q}_r) e_v(\omega) d\omega \quad (23)$$

where F_v , Γ are the positive definite gain matrices, $\hat{\beta}(t)$ and β_0 are the estimate and initial known value of β , respectively, and

$$\dot{q}_r = \dot{q}_d - \Lambda_p e$$

$$\ddot{q}_r = \ddot{q}_d - \Lambda_p \dot{e}$$

$$e_v = \dot{q} - \dot{q}_r$$

$$Y(q, \dot{q}, \ddot{q}_r, \ddot{q}_r) \hat{\beta}(t) = \hat{M}(q) \ddot{q}_r + \hat{C}(q, \dot{q}) \dot{q}_r + \hat{g}(q)$$

where Λ_p is a positive definite gain matrix. Substituting the control law (22) into the free robot dynamics (11) and rearranging terms results in the following error dynamics

$$M(q) \dot{e}_v + C(q, \dot{q}) e_v + F_v e_v = Y(q, \dot{q}, \ddot{q}_r, \ddot{q}_r) \tilde{\beta}(t) \quad (24)$$

where $\tilde{\beta}(t) = \hat{\beta}(t) - \beta$ is the parameter estimation error. Stability of this phase can be shown using Lyapunov's second method and can be found in [18].

3.2 Control During Transition Phase. Transition phase starts when the robot makes its first impact with the surface. Then, we project the desired trajectory into tangential direction of the surface using the tangential projection matrix Q_ϕ . The desired motion trajectory of the robot is developed based on a priori knowledge of the location of the constraint. The first impact gives the actual location of the constraint surface. After the first impact, the desired trajectory is modified such that the desired velocity

and acceleration in normal direction are zero, i.e., $P_\phi \dot{q}_d = 0$. The control law for the transition phase is chosen as follows:

$$\tau = Y(q, \dot{q}, \ddot{q}_r, \ddot{q}_r) \beta - F_v e_v - \lambda_{in} P_\phi \text{sgn}(e_{vn}) \quad (25)$$

where

$$\begin{aligned} \dot{q}_r &= \dot{q}_d - \lambda_p e = Q_\phi \dot{q}_d - \lambda_p e \\ \ddot{q}_r &= \ddot{q}_d - \lambda_p \dot{e} \\ e_v &= \dot{q} - \dot{q}_r \\ e_{vn} &= P_\phi e_v \end{aligned}$$

where λ_{in} and λ_p are positive gains. Substituting the control law into the dynamic equations we obtain the error dynamics

$$M(q) \dot{e}_v + C(q, \dot{q}) e_v + F_v e_v = -\lambda_{in} P_\phi \text{sgn}(e_{vn}) \quad (26)$$

3.3 Stability of Transition Phase. To show stability of the closed-loop system in the transition phase, choose the following Lyapunov function candidate:

$$V(e_v) = \frac{1}{2} e_v^T M(q) e_v \quad (27)$$

Taking the derivative of the Lyapunov function candidate along the trajectories of (26) and simplifying we obtain

$$\begin{aligned} \dot{V}(e_v) &= -e_v^T F_v e_v - \lambda_{in} e_v^T P_\phi \text{sgn}(e_{vn}) \\ &= -e_v^T F_v e_v - \lambda_{in} \|e_{vn}\|_1 \end{aligned} \quad (28)$$

Therefore, from (27) and (28), $V(e_v)$ is indeed a Lyapunov function, i.e., V is positive definite and its time-derivative along the trajectories of (26) is negative definite. Using Lyapunov theorem [33], e_v is bounded. Further since e_v appears explicitly in \dot{V} , e_v converges to zero asymptotically. Notice that from the stability analysis above it is shown that the Lyapunov function decreases between impacts. If a series of impacts is involved during the transition phase, we have to show that the Lyapunov function also decreases after each impact. In the transition phase, assume that robot impacts the constraint surface at time instants t_k , where $k = (1, 2, \dots)$. Let $e_{vk}^+ = e_v(t_k + \delta)$ and $e_{vk}^- = e_v(t_k - \delta)$, where $\delta \rightarrow 0$ under the assumption that the impact duration is infinitesimally small. The difference in Lyapunov function before and after k th impact is evaluated in the following.

$$\begin{aligned} \Delta V_k &= V_k^+ - V_k^- \\ &= \frac{1}{2} (e_{vk}^+)^T M(q) (e_{vk}^+) - \frac{1}{2} (e_{vk}^-)^T M(q) (e_{vk}^-) \\ &= \frac{1}{2} (\dot{q}_k^+ - \dot{q}_{kr})^T M(q) (\dot{q}_k^+ - \dot{q}_{kr}) \\ &\quad - \frac{1}{2} (\dot{q}_k^- - \dot{q}_{kr})^T M(q) (\dot{q}_k^- - \dot{q}_{kr}) \\ &= \frac{1}{2} (\dot{q}_k^+)^T M(q) (\dot{q}_k^+) - \frac{1}{2} (\dot{q}_k^-)^T M(q) (\dot{q}_k^-) \\ &\quad - [(\dot{q}_{kr})^T M(q) (\dot{q}_k^+) - (\dot{q}_{kr})^T M(q) (\dot{q}_k^-)] \end{aligned}$$

Notice that the first term and second term represent the kinetic energy after and before the k th impact, respectively. Using (16) and (14), we obtain

$$\begin{aligned} \Delta V_k &= (KE)_k^+ - (KE)_k^- - (\dot{q}_{kr})^T M(q) (\dot{q}_k^+ - \dot{q}_k^-) \\ &= -(\Delta K)_k - (\dot{q}_{kr})^T M(q) \Delta \dot{q}_k \\ &= -(\Delta K)_k - (\dot{q}_{kd} - \lambda_p e_k)^T f_I \end{aligned}$$

During the transition phase, we have $P_\phi \dot{q}_{kd} = 0$ and $P_\phi e_k = 0$, and thus we obtain

$$\begin{aligned} \Delta V_k &= -(\Delta K)_k - [Q_\phi (\dot{q}_{kd} - \lambda_p e_k)]^T f_I \\ &= -(\Delta K)_k - (\dot{q}_{kd} - \lambda_p e_k)^T Q_\phi^T f_I \end{aligned} \quad (29)$$

The first term in (29) is the kinetic energy reduction at the k th impact. Notice that $Q_\phi^T f_I$ is the tangential force impulse caused by friction. For frictionless impact, $\Delta V_k < 0$ is immediate because f_I lies in the normal direction, i.e., $f_I = P_\phi f_I$, and hence $Q_\phi^T f_I$ is a null vector. In the case of impact with friction, assuming that the position error in the tangential direction is very small, the second term in (29) is approximately the work done by the friction force, which is

$$\dot{q}_{kd}^T Q_\phi^T f_I = \lim_{\Delta t \rightarrow 0} \int_{t_*}^{t_* + \Delta t} \dot{q}_{kd}^T Q_\phi^T J^T(q) f(\omega) d\omega \quad (30)$$

In the above integral, $Q_\phi^T J^T(q) f(\omega)$ is the generalized friction force at impact. The work done by the friction force is smaller than the kinetic energy reduction due to impact. It is reasonable to assume that the approximation given by (30) is smaller than the kinetic energy reduction, $(\Delta K)_k$. Thus, giving the result $\Delta V_k < 0$. Notice that the result is true for the regulation case, i.e., regulating the robot end-effector on the surface, because there is no desired tangential motion, and hence the second term in (29) is zero.

3.4 Motion and Force Control During Surface Finishing.

When the transition phase dies down, i.e., the velocity normal to the surface becomes zero ($P_\phi \dot{q} \rightarrow 0$), then the robot is in stable contact with the surface. At this time we switch to constrained motion control, i.e., motion control in the tangential direction and force control in the normal direction. In this phase it is assumed that the inertial parameters of the robot are estimated during the free motion phase and hence known. During this phase, manipulator dynamics is

$$M(q) \ddot{q} + C(q, \dot{q}) \dot{q} = \tau + v(q) f_n + v'(q) \xi f_n \quad (31)$$

We choose the following control law

$$\tau = M(q) \ddot{q}_r + C(q, \dot{q}) \dot{q}_r - F_v e_v - v(q) f_{nd} - v'(q) \hat{\xi} f_n \quad (32)$$

and the adaptation law for the grinding coefficient as

$$\dot{\hat{\xi}} = -\Gamma_f^{-T} v'^T(q) e_{vf_n} \quad (33)$$

where f_{nd} is the desired normal force, and

$$\begin{aligned} \dot{q}_r &= Q_\phi [\dot{q}_d - \Lambda_p e] + \beta_f \bar{v}(q) e_{vf_n} \\ \ddot{q}_r &= Q_\phi [\ddot{q}_d - \Lambda_p \dot{e}] + \dot{Q}_\phi [\dot{q}_d - \Lambda_p e] + \beta_f \bar{v}'(q) e_{vf_n} + \beta_f \dot{\bar{v}}(q) e_{vf_n} \\ e_v &= \dot{q} - \dot{q}_r \\ \bar{v}(q) &= v(q) / \|v(q)\|^2 \\ e_{fn} &= f_n - f_{nd} \\ e_{vf_n} &= \int_0^t e_{fn}(\omega) d\omega \end{aligned}$$

Substituting the control law (32) into the dynamic equation (31) we obtain

$$M(q) \dot{e}_v + C(q, \dot{q}) e_v + F_v e_v = v(q) e_{fn} + v'(q) \tilde{\xi} f_n \quad (34)$$

where $\tilde{\xi} = \hat{\xi} - \xi$ is the estimation error of the grinding coefficient.

3.5 Stability of Constrained Motion Phase. Closed-loop stability during this phase can be shown using the following Lyapunov function candidate becomes:

$$V(e_v, e_{fn}) = \frac{1}{2} e_v^T M(q) e_v + \frac{1}{2} \beta_f e_{vf_n}^2 + \frac{1}{2} \tilde{\xi}^T \Gamma_f \tilde{\xi} \quad (35)$$

Taking the time derivative of the Lyapunov function candidate along the trajectories of (34), we obtain

$$\begin{aligned}\dot{V}(e_v, e_{fn}) &= e_v^T M(q) \dot{e}_v + \frac{1}{2} e_v^T \dot{M}(q) e_v + \beta_f e_{fn} e_{vfn} + \dot{\xi}^T \Gamma_f \tilde{\xi} \\ &= -e_v^T F_v e_v + e_v^T v(q) e_{fn} + e_v^T v'(q) \tilde{\xi} f_n \\ &\quad + \beta_f e_{fn} e_{vfn} + \dot{\xi}^T \Gamma_f \tilde{\xi}\end{aligned}\quad (36)$$

where we have used the skew-symmetry property of the robot, i.e., $(1/2\dot{M}(q) - C(q, \dot{q}))$ is skew-symmetric. We can simplify the term $e_v^T v(q) e_{fn}$ as follows:

$$\begin{aligned}e_v^T v(q) e_{fn} &= [\dot{q} - \dot{q}_r] v(q) e_{fn} \\ &= [(P_\phi + Q_\phi) \dot{q} - Q_\phi (\dot{q}_d - \Lambda_p e) - \beta_f \bar{v}(q) e_{vfn}]^T v(q) e_{fn} \\ &= [Q_\phi \dot{q} - Q_\phi (\dot{q}_d - \Lambda_p e) - \beta_f \bar{v}(q) e_{vfn}]^T v(q) e_{fn} \\ &= [Q_\phi (\dot{e} - \Lambda_p e) - \beta_f \bar{v}(q) e_{vfn}]^T v(q) e_{fn} \\ &= (\dot{e} - \Lambda_p e)^T Q_\phi^T v(q) e_{fn} - \beta_f e_{vfn} \bar{v}^T(q) v(q) e_{fn} \\ &= -\beta_f e_{vfn} \frac{v^T(q)}{\|v(q)\|^2} v(q) e_{fn} \\ &= -\beta_f e_{vfn} e_{fn}\end{aligned}\quad (37)$$

Notice that we have used $P_\phi(q) \dot{q} = 0$, this is true when the robot end-effector is on the surface. Substituting (37) into the derivative of the Lyapunov function candidate (36), we get

$$\dot{V}(e_v, e_{fn}) = -e_v^T F_v e_v + e_v^T v'(q) \tilde{\xi} f_n + \dot{\xi}^T \Gamma_f \tilde{\xi}\quad (38)$$

Using the adaptation law given by (33) we obtain

$$\dot{V}(e_v) = -e_v^T F_v e_v < 0\quad (39)$$

Therefore, since V is a positive definite function and \dot{V} is negative definite, V given by (35) is a Lyapunov function. Hence the error signals e_v , e_{vfn} , and $\tilde{\xi}$ are bounded. Further, since e_v appears explicitly in \dot{V} , e_v converges to zero asymptotically.

3.6 Overall Stability. Stability of the closed-loop system with the proposed controllers within each phase is shown in the preceding sections. To show that the robot system is stable for the complete task, we consider the complete task as a time concatenation of the three phases. The desired motion trajectory (path DABCD in Fig. 3) is generated based on a priori knowledge of the location of the constraint. In the event of impact, this desired trajectory is projected into the tangential directions of the con-

straint surface. The actual location of the constraint surface is known after the first impact. Regulation problem is considered in the normal direction, i.e., regulation of the tool onto the surface with zero normal velocity. Since the desired trajectory is different in each phase, comparison of the Lyapunov function of one phase from the other is not practical. Notice that the reference velocity error, e_v , in each phase is different, even though we use the same notation for it in each phase. The closed-loop system is shown to be stable within each phase and the robot system states are bounded when switching from one phase to another. Hence, stability concept similar to the one given by lemma 8.3 of [24] can be used for the proposed framework.

4 Experimental Platform

The robotic surface finishing system consists of a two-link robot system, computer for real-time control, force sensor, surface finishing tool, and a constraint fixture. Figure 2 illustrates the complete hardware platform of the robotic surface finishing system. The main part of the system is a two-axis direct drive manipulator, which is shown in Fig. 2. Each axis is driven by an NSK Megatorque direct drive servo-motor which is capable of up to 3 revolutions per second maximum velocity and position feedback resolution of up to 156,400 counts per revolution. The base motor delivers up to 245 N-m of torque output, and the elbow motor produces up to 40 N-m torque output. The NSK Megatorque motor consists of a high torque direct drive brushless actuator, a high-resolution brushless resolver, and a heavy duty precision bearing. The Megatorque motor is capable of producing extremely high torque at low speeds suitable for direct drive applications. The heavy-duty bearing eliminates the need for separate mechanical support since the motor case can often support the load directly. The direct drive actuator eliminates the need for gear reduction, so repeatability is limited only by the resolution of the position feedback. Also, direct coupling of the motor and load in comparison to flexible couplings permits tighter and more direct control of the load.

The dynamic model of the manipulator in joint space is given by

$$M(q) \ddot{q} + C(q, \dot{q}) \dot{q} = \tau + J^T f\quad (40)$$

where $M(q)$ is the inertia matrix given by

$$M(q) = \begin{bmatrix} p_1 + 2p_3 c_2 & p_2 + p_3 c_2 \\ p_2 + p_3 c_2 & p_2 \end{bmatrix}\quad (41)$$

and $C(q, \dot{q})$ is the Coriolis matrix given by

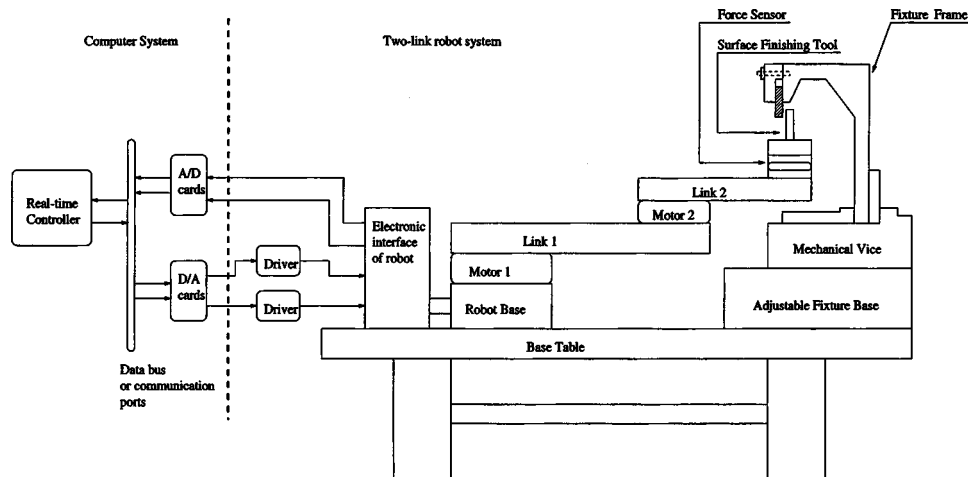


Fig. 2 Schematic of robotic surface finishing system

$$C(q, \dot{q}) = \begin{bmatrix} -2\dot{q}_2 p_3 s_2 & -\dot{q}_2 p_3 s_2 \\ \dot{q}_1 p_3 s_2 & 0 \end{bmatrix} \quad (42)$$

where $c_2 = \cos(q_2)$, $s_2 = \sin(q_2)$ and p_1, p_2, p_3 are the coupled manipulator inertial parameters, whose true values are 3.25, 0.12, 0.20, respectively. The mass matrix, $M(q)$, and Coriolis matrix, $C(q, \dot{q})$, are linear in terms of the coupled manipulator inertial parameters. Hence the left-hand side of (40) can be written as

$$M(q)\ddot{q} + C(q, \dot{q})\dot{q} = Y(q, \dot{q}, \ddot{q})\beta$$

where $\beta = [p_1, p_2, p_3]^T$, and $Y(q, \dot{q}, \ddot{q})$ is given by

$$Y(q, \dot{q}, \ddot{q}) = \begin{bmatrix} \ddot{q}_1 & \ddot{q}_2 & c_2(2\ddot{q}_1 + \ddot{q}_2) - \dot{q}_2(2\dot{q}_1 + \dot{q}_2)s_2 \\ 0 & \ddot{q}_1 + \ddot{q}_2 & \ddot{q}_1 c_2 + \dot{q}_1^2 s_2 \end{bmatrix}$$

The computer system consists of the direct drive manipulator controller (host computer), servo DSP and I/O cards associated with the sensors. The overall system consists of three processors: host Pentium processor, servo DSP (TMS320C30), force sensor DSP. The host processor is used for reference generation, user interface, and coordination of other processors. Real-time control is performed using servo DSP. Force sensor DSP is used for filtering of raw force data, tool offset calculation, and force data processing. The three processor architecture provides flexibility in terms of collecting force data from the force sensor and position/velocity data from the motor resolvers at different sampling rates.

The real-time computation load is distributed to three CPUs. Force signal processing modules runs on force sensor DSP. Host CPU acts as a user interface, coordinates data flow among software modules, handles real-time data communication, performs safety checks and "housekeeping functions." Servo DSP is reserved only for servo control modules. The force sensor system is capable of sampling frequency of up to 4 kHz. The servo DSP (TMS320C30) is capable of finishing 33.3 million floating-point computations per second. The minimum sampling time which can be implemented is determined by the amount of time required for the host computer to perform interprocessor communication, which is approximately 500 micro-seconds. Since a maximum of 60 nano-seconds is required for a single TMS320C30 machine instruction, complex control algorithms which are hundreds of lines long can be executed. A servo sampling frequency of 250 Hz is used in all the experiments.

5 Experimental Results

Experiments using the proposed controller were conducted for both surface following and surface finishing. In the surface following experiments, a smooth cylindrical metal tip/probe is used as an end-effector. The desired trajectory is a complete task containing both free motion and constrained motion. Stability problems are encountered when switching from free motion to constrained motion in the presence of constraint uncertainty. Surface following experiments were conducted with different levels of constraint uncertainty and different speeds of travel on the surface. Experiments were also conducted to test the effects of constraint rigidity on tracking performance. Robotic surface finishing experiments consist of chamfering of the straight edge of a surface. In these experiments a cutting tool is used instead of a smooth metal tip/probe for material removal. Similar to up and down milling in machining, robotic surface finishing operations can be categorized into two types depending on the tool rotation and direction of travel of the tool on the surface. Chamfering experiments were conducted to study the effect of these two types.

The constraint surface $\phi(q)$ is a thick straight aluminum sheet firmly held by a vice. The desired complete task for the robot is to move towards the constraint surface, make contact with the surface, follow the surface while maintaining a desired normal contact force, and leave the surface to return to the starting point.

Figure 3 shows the desired trajectory of the robot **CDABC** and

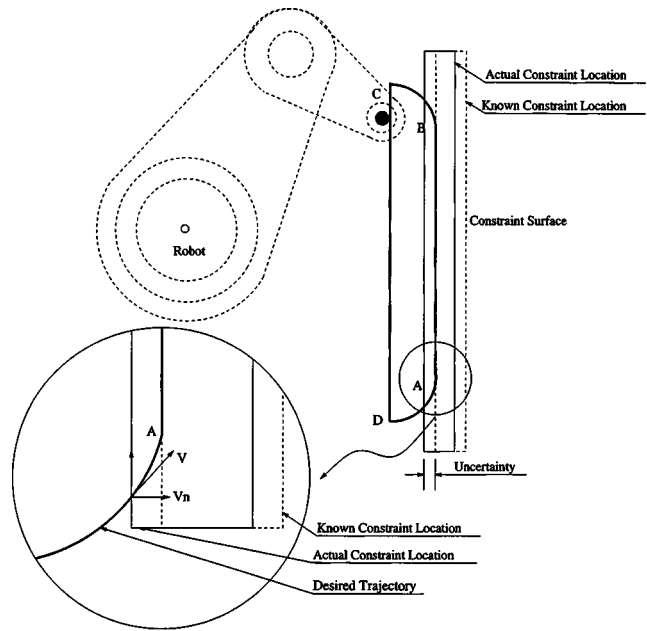


Fig. 3 Transition due to constraint uncertainty

also the different phases of motion along the desired trajectory. Notice that at **A** the robot may impact the constraint due to constraint uncertainty. Desired trajectory is designed such that without any uncertainty in the location of the constraint, the robot lands on the surface smoothly, i.e., there is no normal velocity at contact. The desired velocity of the robot end-effector in Cartesian coordinates during constrained motion, i.e., along **AB**, is chosen to be a constant to obtain steady feedrate during surface finishing. Also, the desired trajectory is such that the entire task **CDABC** is completed in 12 seconds. Control sampling period of 4 milliseconds and force data sampling period of 0.5 milliseconds. Experiments are categorized into the following two groups: (1) Surface following experiments and (2) Surface finishing experiments.

5.1 Surface Following Experiments. In this set of experiments, surface following is conducted during constrained motion phase to test the control strategy without material removal. The main focus is on transition control. Three factors affecting transition phase were considered: (i) constraint uncertainty; (ii) desired velocity; (iii) rigidity of the surface. For all the surface following experiments, the feedback gains are kept the same. The desired normal force value is taken to be 45 N. Fig. 3 shows the nonzero normal velocity due to constraint uncertainty. In the experiments, when the robot makes its first impact, the desired trajectory is modified such that the desired velocity and acceleration normal to the surface are zero.

In the first group of experiments, we implement direct switching from free motion phase to constrained motion phase without any transition control. Experimental results of three typical cases are shown in Fig. 4: (1) $\zeta = 5.0$ mm, $v = 0.07$ m/s, and normal constraint rigidity; (2) $\zeta = 5.0$ mm, $v = 0.14$ m/s, and normal constraint rigidity; (3) $\zeta = 5.0$ mm, $v = 0.07$ m/s, and high constraint rigidity. Normal position error and normal force of three cycles are given in Fig. 4. In the first case, the tool tip bounces on the surface and large impact forces occur immediately after contact due to non-zero normal velocity. It is observed that the bounces become more significant when the velocity or constraint rigidity is increased. In the case of higher speed, the velocity of impact is also larger and hence the bounces occur over a longer period of time when compared to the lower speed case. Also, notice that the peak of the impact force has not changed significantly due to

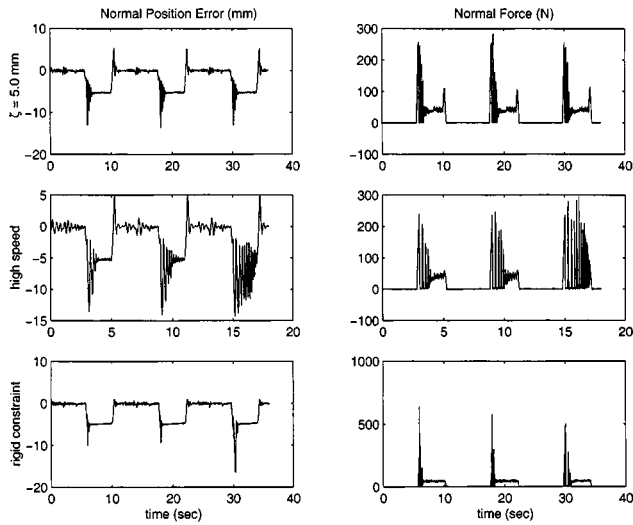


Fig. 4 Surface following results using direct switch

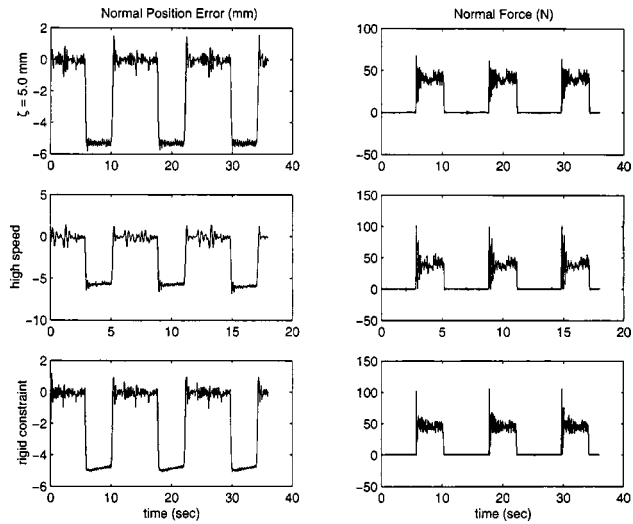


Fig. 5 Surface following results using transition control

change in speeds, this may be due to constraint compliance. For rigid constraint case, the peak impact force is larger but fewer bounces are observed.

Extensive experiments with various constraint uncertainties, feedrate, and rigidity of constraint have been conducted using the proposed transition controller. Figure 5 shows that the results using the transition controller are much improved when compared with experimental results without transition control (Fig. 4). Tables 1 and 2 give a comparison summary of the surface following experiments. These tables show that the peak impact force and the number of bounces are reduced with transition control. The effectiveness of the transition controller and control switching strategy is validated by the experimental results.

Same set of control and estimation gains are used in each experiment. The gains are given below.

$$F_v = \begin{bmatrix} 10 & 0 \\ 0 & 10 \end{bmatrix} \quad \Lambda_p = \begin{bmatrix} 20 & 0 \\ 0 & 15 \end{bmatrix} \quad \Gamma = \begin{bmatrix} 2.0 & 0 & 0 \\ 0 & 0.2 & 0 \\ 0 & 0 & 0.2 \end{bmatrix}$$

The initial values of manipulator inertial parameters were chosen as: $p_{10}=1.0$; $p_{20}=0.1$; $p_{30}=0.1$. The estimated values after the free motion phase are: $\hat{p}_1=2.8$; $\hat{p}_2=0.15$; $\hat{p}_3=0.19$, which are close to the true values. For the transition phase, $\lambda_{in}=0.6$ and $\lambda_p=15$. The normal force feedback gain is $\beta_f=0.01$ during the constrained motion phase.

5.2 Surface Finishing Experiments. In this section, experimental results of surface finishing experiments are given. For all the experiments in this section the desired force is $f_{nd}=15$ N. Similar to up and down milling in machining, a robotic surface finishing operation can be categorized into two modes depending on the tool rotation and the direction of travel of the tool mounted on the robot end-effector. The two modes are illustrated in Fig. 6 and Fig. 7. For mode 1, the normal force f_n caused by surface finishing process pushes the tool away from the surface, in contrast, the normal force holds the tool on the surface in mode 2. Hence, more stable contact can be achieved in mode 2. In mode 1, the tangential force, f_t , is in the same direction as the tangential motion along the surface. In mode 2, f_t is in the opposite direction of motion. Hence, the magnitude and sign of the coefficient of grinding friction, ξ in cutting force model are different for mode 1 and 2. For the experimental results in this paper, the grinding

Table 1 Summary of transition control experiments [normal force peak] (N)

	$v=0.14$ m/s Normal rigidity		$v=0.07$ m/s Normal rigidity		$v=0.07$ m/s High rigidity	
	Direct switch	Transition control	Direct switch	Transition control	Direct switch	Transition control
Constraint uncertainty						
0.0 mm	62.3	56.1	73.73	56.4	67.1	62.5
2.5 mm	101.5	63.5	136.9	52.4	270.6	81.5
5.0 mm	293.8	101.3	282.8	67.9	639.5	105.7
7.5 mm	no data	104.0	no data	65.5	no data	no data

Table 2 Summary of transition control experiments [number of bounces]

	$v=0.14$ m/s Normal rigidity		$v=0.07$ m/s Normal rigidity		$v=0.07$ m/s High rigidity	
	Direct switch	Transition control	Direct switch	Transition control	Direct switch	Transition control
Constraint uncertainty						
0.0 mm	0	0	0	0	0	0
2.5 mm	2	0	2-3	0	5 or more	1
5.0 mm	4-15	1	4	0	5 or more	1
7.5 mm	no data	1	no data	0	no data	no data

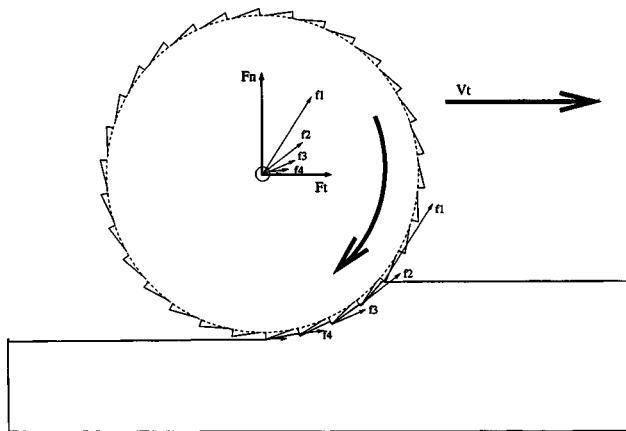


Fig. 6 Surface finishing mode 1

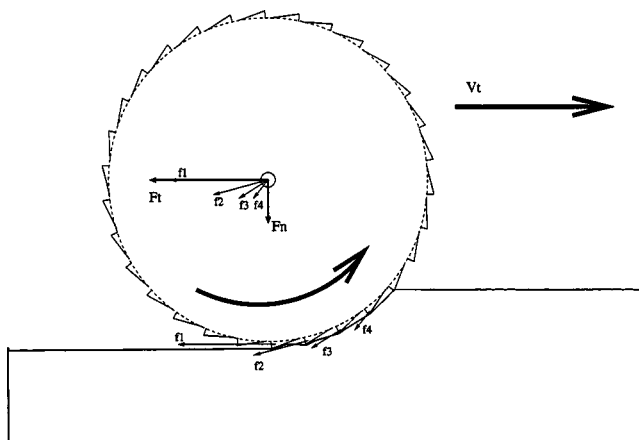


Fig. 7 Surface finishing mode 2

coefficient is -0.8 when robot works in mode 1 and 1.5 when it is in mode 2. All other gains are same as surface following experiments.

Surface finishing experiments were conducted in both mode 1 and mode 2 with different work piece location uncertainty. Experimental results of mode 1 are shown in Fig. 8 and Fig. 9.

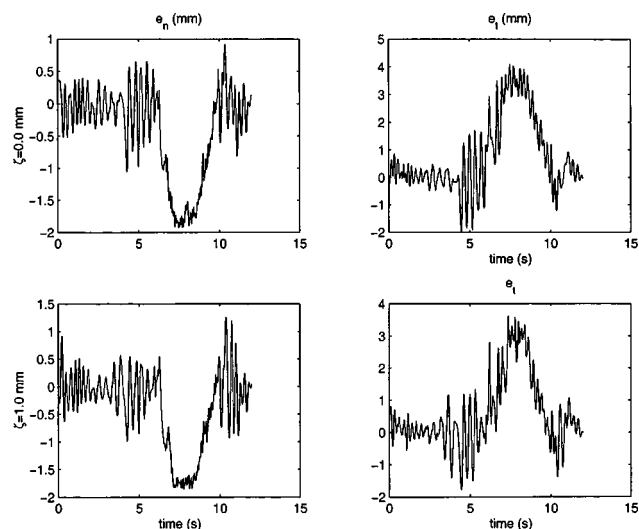


Fig. 8 Tracking errors during surface finishing, mode 1

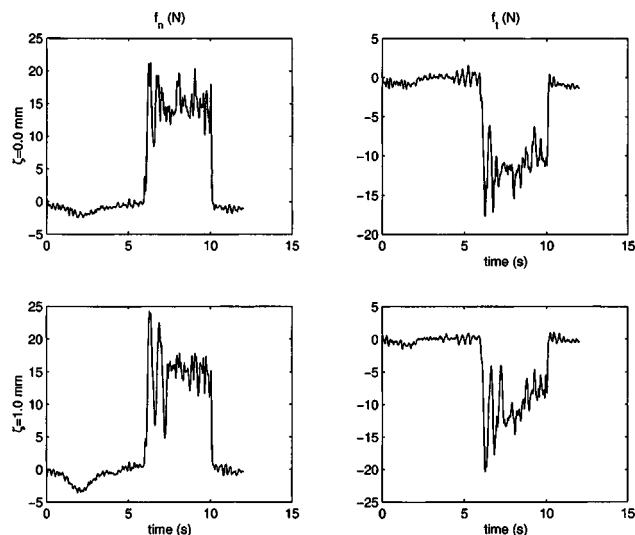


Fig. 9 Forces regulation during surface finishing, mode 1

Figure 8 contains normal and tangential position tracking errors with constraint uncertainty $\zeta=0$ and $\zeta=1$ mm. During the surface finishing process, given by time interval between 6 and 10 seconds on the plots, the compliance of the tool contributes to the normal tracking error. Stable contact is achieved. Figure 9 shows that normal force is regulated at the desired level 15 N during surface finishing. Constraint uncertainty causes a larger peak force and oscillations when the tool makes contact with the surface.

Experimental results of mode 2 are shown in Fig. 10 and Fig. 11. Figure 10 indicates that the normal position tracking error of mode 2 is similar to that of mode 1. However, the tangential tracking error is different from that of mode 1. This is due to different tangential force direction of mode 1 and mode 2. Figure 11 shows that normal forces are regulated at the desired level of 15 N during surface finishing with and without constraint uncertainty. It should be observed that peak normal force and force oscillation when contact is made are not significant in mode 2.

Stable contact and normal force regulation is achieved in both surface finishing modes using the proposed control strategy. Comparing experimental results of mode 1 and mode 2 indicates that better surface finish can be obtained in mode 2. Figure 12 and Fig. 13 give the discrete FFT of normal and tangential force signals.

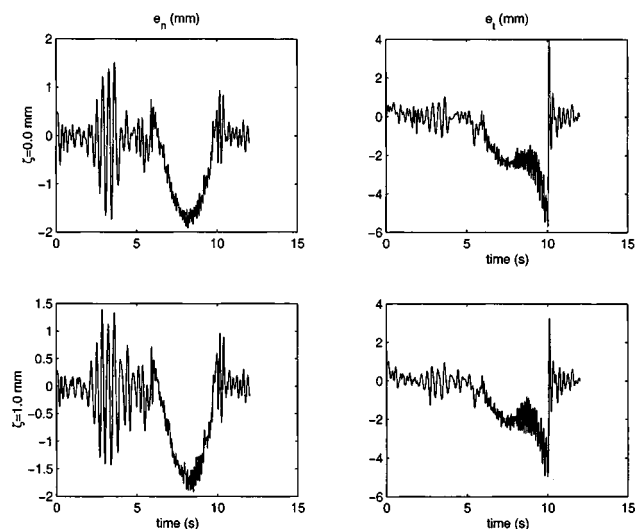


Fig. 10 Tracking errors during surface finishing, mode 2

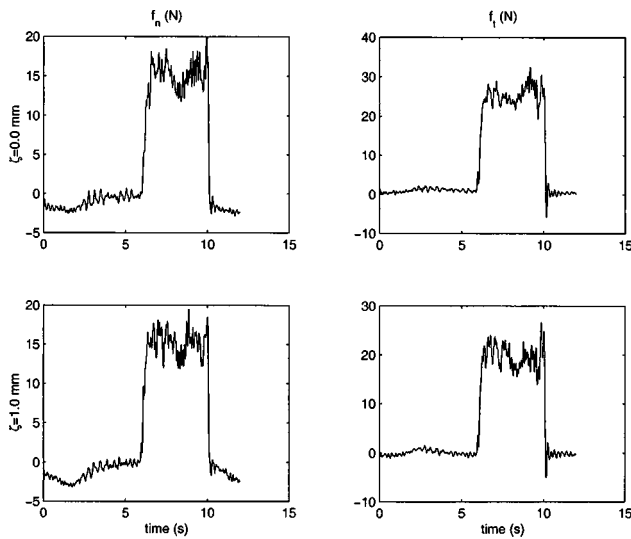


Fig. 11 Forces regulation during surface finishing, mode 2

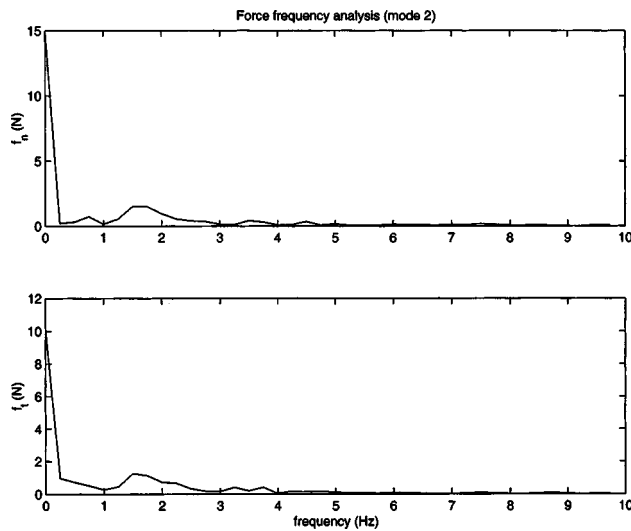


Fig. 12 FFT of force data, mode 1

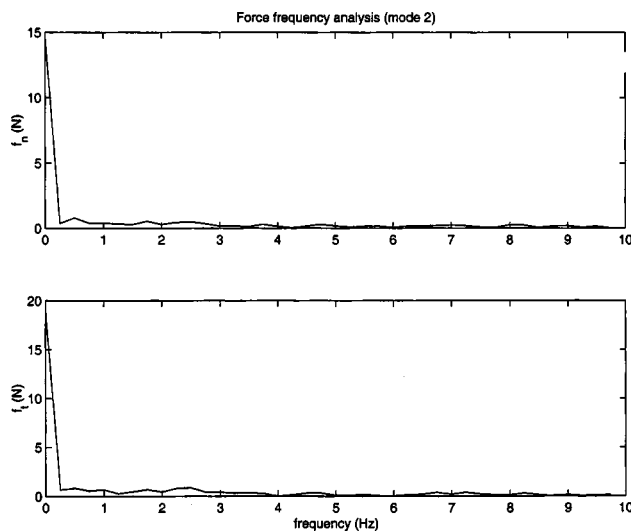


Fig. 13 FFT of force data, mode 2

Normal forces of mode 1 and mode 2 all contain DC component whose magnitude is 15 N. (This implies that force normal to the surface is regulated at desired level for all cases. Also, the tangential forces are kept at a constant level determined by the value of ξ .) Since the magnitude of f_t may be larger than that of f_n , tangential force compensation becomes critical in obtaining the necessary material removal and surface finish. For mode 1, noise components around 1.5 Hz are observed. In contrast, no significant noise component in f_n and f_t signals are observed in mode 2.

6 Conclusions

In this paper, we have developed a dynamic model for robots performing a surface finishing operation. The dynamic model consists of three phases of motion: free motion phase, transition phase, and constrained phase. Control algorithm for each phase is designed. In the transition phase, a discontinuous control algorithm is proposed, which is shown to be asymptotically stable. In the constrained motion phase, the robot model includes both the tangential force that is due to material removal and normal force to keep the robot end-effector on the surface. Assuming steady feed-rate during the constrained motion, the magnitude of the tangential force and the normal force are related by the coefficient of grinding friction. Hence, the dynamic model in the constrained phase includes both the tangential forces and normal forces. A gradient-type adaptation algorithm is proposed to estimate the coefficient of grinding friction. Extensive experiments were conducted to verify the performance of the proposed control strategy for both surface following and surface finishing operations. Experimental results show much improved performance of the proposed control strategy when compared with the results available in literature. Our future work will focus on more experiments in robotic polishing. In this work, grinding model that relates normal and tangential force by constant coefficient of grinding friction has been used. A constant coefficient of grinding friction has been used in the experiments to compensate for tangential forces that arise due to material removal. In the future, we will focus on other models and also on-line estimation of the coefficient of grinding friction.

References

- [1] Ramachandran, N., Pande, N., and Ramakrishnan, N., 1994, "The Role of Deburring in Manufacturing: A State-of-the Art Survey," *J. Mater. Process. Technol.*, **44**.
- [2] Proctor, F. M., and Murphy, K. N., 1989, "Advanced Deburring System Technology," *Keynote Address at the ASME Winter Annual Meeting*, San Francisco, CA.
- [3] Komanduri, R., Merchant, M. E., and Shaw, M. C., 1993, "Symposium on US Contributions to Machining and Grinding Research in the 20th Century," NSF Sponsored Symposium (Organizer: R. Komanduri), *Appl. Mech. Rev.*, **46**, No. 3.
- [4] Stouffer, K. A., Russel, R., Jr., Archacki, R., Engel, T., Dansereau, R., and Grot, A., 1997, "Advanced Deburring and Chamfering System (ADACS): Final Report," NIST Technical Report NISTIR 5915.
- [5] Koelsch, J. R., 1990, "Banish Manual Deburring," *Manuf. Eng.*, pp. 71–75.
- [6] Erickson, E. G., 1991, "Automated Robotic Deburring Produces Quality Components," *Automation*, March, pp. 50–51.
- [7] Dornfeld, D. A., 1995, "Consortium on Deburring and Edge Finishing (CODEF) News," Laboratory for Manufacturing Automation, University of California, Berkeley, CA.
- [8] Kazerooni, H., 1988, "Robotic Deburring of Two-dimensional Parts with Unknown Geometry," *J. Manuf. Syst.*, **7**, No. 4, pp. 329–338.
- [9] Bone, G. M., Elbestawi, M. A., Lingarkar, R., and Liu, L., 1991, "Force Control of Robotic Deburring," *ASME J. Dyn. Syst., Meas., Control*, **113**, pp. 395–400.
- [10] Whitney, D. E., 1977, "Force Feedback Control of Manipulators," *ASME J. Dyn. Syst., Meas., Control*, **102**, pp. 91–97.
- [11] Raibert, M. H., and Craig, J. J., 1981, "Hybrid Position/Force Control of Manipulators," *ASME J. Dyn. Syst., Meas., Control*, **102**, pp. 126–133.
- [12] Whitney, D. E., 1982, "Quasi-static Assembly of Compliantly Supported Rigid Parts," *ASME J. Dyn. Syst., Meas., Control*, **104**, pp. 65–77.
- [13] Mason, M. T., 1981, "Compliance and Force Control of Computer Controlled Manipulators," *IEEE Trans. Syst. Man Cybern.*, **SMC-11**, No. 6, pp. 418–432.

- [14] Hogan, N., 1985, "Impedance Control: An approach to manipulation: Part I-Theory; Part II-Implementation; Part III-Applications," *ASME J. Dyn. Syst., Meas. Control*, **107**, pp. 1–24.
- [15] Kazerooni, H., Sheridan, T., and Houpt, P., 1986, "Robust Compliant Motion for Manipulators," *IEEE J. Rob. Autom.*, **2**, No. 2, pp. 83–105.
- [16] Hemami, H., and Wyman, B. F., 1979, "Modeling and Control of Constrained Dynamic Systems with Application to Biped Locomotion in the Frontal Plane," *IEEE Trans. Autom. Control*, **24**, pp. 526–535.
- [17] McClamroch, N. H., 1986, "Singular Systems of Differential Equations as Dynamic Models for Constrained Robot System," *IEEE International Conference on Robotics and Automation*, pp. 21–28.
- [18] Arimoto, S., 1996, *Control Theory of Non-linear Mechanical Systems—A Passivity-Based and Circuit-Theoretic Approach*, Oxford, New York.
- [19] Wang, D., and McClamroch, N. H., 1993, "Position and Force Control for Constrained Manipulator Motion: Lyapunov's Direct Method," *IEEE Trans. Rob. Autom.*, **9**, No. 3, pp. 308–312.
- [20] Mills, J. K., and Lokhorst, D. M., 1993, "Stability and Control of Robotic Manipulators During Contact/Noncontact Task Transition," *IEEE Trans. Rob. Autom.*, **9**, No. 3, pp. 335–346.
- [21] Youcef-Toumi, K., and Gutz, D. A., 1994, "Impact and Force Control: Modeling and Experiments," *ASME J. Dyn. Syst., Meas., Control*, **116**, pp. 89–98.
- [22] Pagilla, P. R., and Tomizuka, M., 1997, "Contact Transition Control of Non-linear Mechanical Systems Subject to a Unilateral Constraint," *ASME J. Dyn. Syst., Meas., Control*, **119**, pp. 749–759.
- [23] Tarn, T. J., Wu, Y., Xi, N., and Isidori, A., 1996 "Force Regulation and Contact Transition Control," *IEEE Control Systems*, pp. 32–40, Feb.
- [24] Brogliato, B., 1996, *Nonsmooth Impact Mechanics: Models, Dynamics, and Control*, Springer-Verlag, London.
- [25] Tornambe, A., 1999, "Modeling and control of the impact in mechanical systems: Theory and experimental results," *IEEE Trans. Autom. Control*, **44**, No. 2, pp. 294–309.
- [26] ten Dam, A. A., Dwarshuis, E., and Willems, J. C., 1997, "The contact problem for linear continuous time dynamical systems: a geometric approach," *IEEE Trans. Autom. Control*, **42**, No. 4, pp. 458–472, Apr..
- [27] van der Schaft, A. J., and Schumacher, J. M., 1998, "Complementarity Modeling of Hybrid Systems," *IEEE Trans. Autom. Control*, **43**, No. 4, pp. 483–499.
- [28] van der Schaft, A. J., and Schumacher H., 2000, *An Introduction to Hybrid Dynamical Systems*, Springer-Verlag, New York.
- [29] Stoianovici, D., and Hurmuzlu, Y., 1996, "A Critical Study of the Applicability of Rigid-Body Collision Theory," *ASME J. Appl. Mech.*, **63**, pp. 307–316.
- [30] King, R., and Hahn, R., 1986, *Handbook of Modern Grinding Technology*, Chapman and Hall.
- [31] Brach, R. M., 1991, *Mechanical Impact Dynamics: Rigid Body Collisions*, Wiley, NY.
- [32] Kozlov, V. V., and Treschev, D. V., 1991, "Billiards: A Genetic Introduction to the Dynamics of Systems with Impacts," *AMS Translations of Mathematical Monographs*, Providence, RI.
- [33] Vidyasagar, M., 1978, *Nonlinear System Analysis*, Prentice Hall, Englewood Cliffs, NJ.